Environmental Pollution 272 (2021) 116002

Contents lists available at ScienceDirect

Environmental Pollution

journal homepage: www.elsevier.com/locate/envpol

Abundant sediment organic matter potentially facilitates chemical iron reduction and surface water blackness in a Chinese deep lake☆

Biao Li [a, b], Muhua Feng [a, *], Xiangchao Chen [c], Yarui Wang [a, b], Yue Shen [a, b], Qinglong L. Wu [a, d]

[a] State Key Laboratory of Lake Science and Environment, Nanjing Institute of Geography and Limnology, Chinese Academy of Sciences, Nanjing, 210008, China
[b] University of Chinese Academy of Sciences, Beijing, 100039, China
[c] Shanghai Tingying Environmental Technology Co., Ltd, Shanghai, 201707, China
[d] Sino-Danish Centre for Education and Research, University of Chinese Academy of Sciences, Beijing, 100039, China

ARTICLE INFO

Article history:
Received 9 July 2020
Received in revised form
21 October 2020
Accepted 3 November 2020
Available online 7 November 2020

Keywords:
Black bloom
Ferrous monosulfide
Organic detritus
Diffusive gradients in thin films (DGT)

ABSTRACT

Black bloom has become an increasingly severe environmental and ecological problem in lots of lakes. Ferrous monosulfide (FeS), which is closely related to chemical iron reduction (CIR), is considered the major cause for black water in shallow lakes, but few studies focus on the effect of organic matters (OM) content on iron and sulfate reduction and its contribution to the black bloom in deep lakes. Here, in Lake Fuxian, a Chinese deep lake which has also suffered from black bloom, FeS was identified responsible for the surface water blackness by using multiple microscopy and element analyses. Dissolved oxygen (DO) penetrated 1.6–4.2 mm in all sediment sites, further indicating FeS formed in the sediments instead of the permanently oxic water column. Geochemical characteristics revealed by diffusive gradients in thin films (DGT) showed that DGT-Fe^{2+} concentration was 57.6–1919.4 times higher than the DGT-S^{2-} concentration and both were positively correlated with DGT-PO_4^{3-}. Combining DGT profiles and anaerobic OM remineralization rate according to bag incubation, iron reduction is more effective than sulfate reduction although the two processes coexisted. Moreover, correlation of DGT-Fe^{2+} and DGT-PO_4^{3-} was better than that of DGT-PO_4^{3-} and DGT-S^{2-} at OM-depleted sites but opposite at OM-rich sites. In addition, total organic carbon (TOC) was significantly positively related to acid volatile sulfide (AVS). We therefore conclude that abundant OM potentially exacerbate chemical iron reduction and further lead to surface water blackness. Our study revealed the mechanisms behind the black bloom and gives credence to the management strategy of reducing OM loading to protect water quality in deep lakes.

Credit author statement

Biao Li, Conceptualization, Investigation, Writing - original draft Muhua Feng, Writing - review & editing, Funding acquisition, Project administration Xiangchao Chen, Investigation, Methodology Yarui Wang, Investigation, Methodology Yue Shen, Writing - original draft Qinglong L Wu, Resources, Supervision.

1. Introduction

In recent years, the black bloom phenomenon identified by conditions wherein water bodies turn black has become an increasingly severe environmental and ecological problem in lakes all over the world (Cao et al., 2020). For example, black water was observed just below the top of the chemocline in Lower Mystic Lake in Massachusetts, USA (Duval and Ludlam, 2001). Several square kilometers of black water have been observed in Germany's Wadden Sea, which was considered a highly dynamic and oxic environment (Freitag et al., 2003). In China, this problem is also very serious as the black bloom problem has been reported in 1861 waterbodies from 218 cities affecting 266 lakes and ponds (Cao et al., 2020) such as Lake Taihu (Feng et al., 2014; Liu et al., 2015; Shen et al., 2013). The problem of black water, likely caused by

☆ This paper has been recommended for acceptance by Dr. Jörg Rinklebe.

* Corresponding author. State Key Laboratory of Lake Science and Environment, Nanjing Institute of Geography and Limnology, Chinese Academy of Sciences, 73 East Beijing Road, Nanjing, 210008, China.
E-mail address: mhfeng@niglas.ac.cn (M. Feng).

https://doi.org/10.1016/j.envpol.2020.116002
0269-7491/

nutrient overload and the outbreak of algal bloom has drawn widespread attention from a concerned public and governmental administrators (Huisman et al., 2018). A common goal of all those involved in eutrophic research is to identify the key factors contributing to black bloom with the ultimate aim of its elimination.

The blackness of water during black bloom is closely associated with metal ions and sulfide (S^{2-}) coupling in sediments (Han et al., 2015; Liu et al., 2015; Wang et al., 2014; Zhou et al., 2021). Because the activity of ferrous iron (Fe^{2+}) is higher than manganous ions (Mn^{2+}), copper ions (Cu^{2+}) and other metal ions, Fe^{2+} can rapidly combine with S^{2-} to form ferrous monosulfide (FeS), which is considered primarily responsible for the blackness of water (Chen et al., 2017). In natural sediment conditions, the formation of Fe^{2+} and S^{2-} are tightly related to organic matters (OM) remineralization coupled to the reduction of an array of electron acceptors (Beulig et al., 2018; Lovley, 1987; Reeburgh, 1983; Thomsen 2004). Specifically, after degradation in the water column and eventually traveling downward to settle on the surface sediment, OM easily leads to dissolved oxygen (DO) consumed near the sediment-water interface (SWI) (Chen et al., 2016; Shen et al., 2013). When nitrate (NO_3^-), nitrite (NO_2^-) and manganese oxides (Mn(IV)) are depleted, ferric oxides (Fe(III)) are reduced by two competitive pathways: one is the microbial iron reduction (MIR, Eq (1)) coupled with OM as the electron donor; the other path is chemical iron reduction (CIR, Eq (2)) coupled with S^{2-} as the electron donor which is produced by sulfate (SO_4^{2-}) reduction.

$$4FeOOH + CH_2O + 8H^+ = CO_2 + 4Fe^{2+} + 7H_2O \quad (1)$$

$$2FeOOH + 3H_2S = 2FeS + S^0 + 4H_2O \quad (2)$$

The chemical iron reduction process produces solid FeS which can contribute to the black bloom instead of the dissolved Fe^{2+} created by MIR (Melton et al., 2014). Throughout the OM remineralization process, microorganisms convert complex OM to smaller molecular OM like acetate and methanol, which can be utilized by methanogens in the terminal process to produce methane (CH_4) (Berberich et al., 2019; Dean et al., 2018). From a thermodynamic perspective, OM pathways are coupled in sequence with different electron acceptors along sediment redox zonation due to competition for substrates. However, different reduction processes coupled with various electron acceptors may also coexist and even overturn (Thomsen et al., 2004), such as iron and sulfate reduction (Canfield et al., 1993; Bethke et al., 2011). In a laboratory study, adding H_2, acetate, or a mixture of fatty acids could promote iron and sulfate reduction and alleviate the competition between the two processes (Achtnich et al., 1995), which may due to the changes in the structure of the microbial community (Chen et al., 2020). A recent study indicated that the relative abundance of iron and sulfur oxidizing bacteria decreased by 47–48% but sulfate reducing bacteria increased by 13% after black bloom, with some protein-like organic matters releasing (Zhou et al., 2021). Sulfate reduction could also occur prior to iron reduction in a low sulfate but abundant OM environment with highly crystalline ferric oxides that are difficult to be utilized by microorganisms (Bethke et al., 2011). Moreover, increasing terrestrial OM potentially enhances CH_4 emission even in oxic surface water (Zhou et al., 2018). These studies indicate abundant OM can facilitate co-occurrence of different OM remineralization pathways mediated by the various microorganisms (Mahmoudi et al., 2020). Consequently, it is reasonable to infer that abundant sediment OM could lead to the co-existence of iron and sulfate reduction which may further facilitate chemical iron reduction and contribute to surface water blackness.

Most of the previously studies focused on the interaction of iron and sulfate reduction, internal phosphorus release and microbial community during black bloom (Chen et al., 2020; Han et al., 2015; Liu et al., 2015; Shen et al., 2013; Yu et al., 2017; Zhou et al., 2021). However, the effect of OM content on iron and sulfate reduction and its contribution to the outbreak of black bloom is still enigmatic. In addition, most reported black bloom studies focus on shallow eutrophic lakes which are dynamic and oxic in the water column (Han et al., 2015; Liu et al., 2015; Shen et al., 2013). Very few have focused on deep lakes, where the stratification period exists and the thermocline forms a barrier that blocks the exchange between the epilimnion and the hypolimnion water (Li et al., 2020). As the deep lakes also face the risks of intense phytoplankton blooms or other water quality problems since the 1980s, the studies of the relationships between OM input and black bloom in deep lakes are not only necessary but also very urgent. (Ho et al., 2019; Huisman et al., 2018; Qin et al., 2020).

Here, the effect of OM content on Fe(III)/SO_4^{2-} reduction and its potential contribution to the black bloom were studied in Lake Fuxian, a Chinese deep oligotrophic lake which has also suffered black water even during stratification period. Our hypotheses are (1) Metal sulfide is still responsible for the surface water blackness during stratification period; (2) abundant OM leads to the coexistence of iron and sulfate reduction, resulting to the increase of chemical iron reduction which contribute to the black bloom. In order to verify the hypotheses above, multiple microscopy and element analyses were used to identify the composition of the black substances, then diffusive gradients in thin films (DGT) and geochemical measurements were applied to characterize the iron, sulfate and phosphate (Fe^{2+}/S^{2-}/PO_4^{3-}) distribution in porewater as well as iron and sulfur species in sediments. Finally, anaerobic OM remineralization rates including iron and sulfate reduction were measured in two sites with different OM contents by bag incubation. On the basis of the data above, the effect of OM content on iron and sulfate reduction and its potential contribution to the surface black water were assessed. Our study will improve the knowledge of the mechanism behind the black bloom and provide scientific basis for the protection of deep lakes and reservoirs.

2. Materials and method

2.1. Study area and sample handling

Lake Fuxian is a typical rift lake with a maximum depth of 155 m and an average depth of 95 m on the border of Chengjiang, Huaning and Jiangchuan County, Yunnan Province, Southwest China. The lake is surrounded by mountains with altitude of 1500–2500 m. It is distributed in a ladder shape with higher altitude in the northern and western basin, and lower altitude in the southern and the eastern basin. The lake water is mainly supplied by rainfall with only few mountain streams, causing the water exchange period is up to 167 years (Nanjing Institute of Geography and Limnology, 1990). Forestland is the dominant land use type around Lake Fuxian and corresponds to 48.3% of the basin area, followed by cultivated land (32.2%), grassland (10.8%) and construction land (8.7%) (Table S1; Zhao et al., 2020). Thermal stratification generally occurs from March to November and overturn usually occurs from December to February in the next year (Li et al., 2020).

Although still with the oligotrophic state, intensive human activities have increased risk of eutrophication in Lake Fuxian (Zhang et al., 2015b). In September 2011, June 2014 and July 2016, exactly during stratification period, some black substances appeared on many sides of the lake lasting for several days (Fig. 1a), and posed a great threat to local drinking water safety. Here, seven sampling sites with diverse OM contents were selected based on two

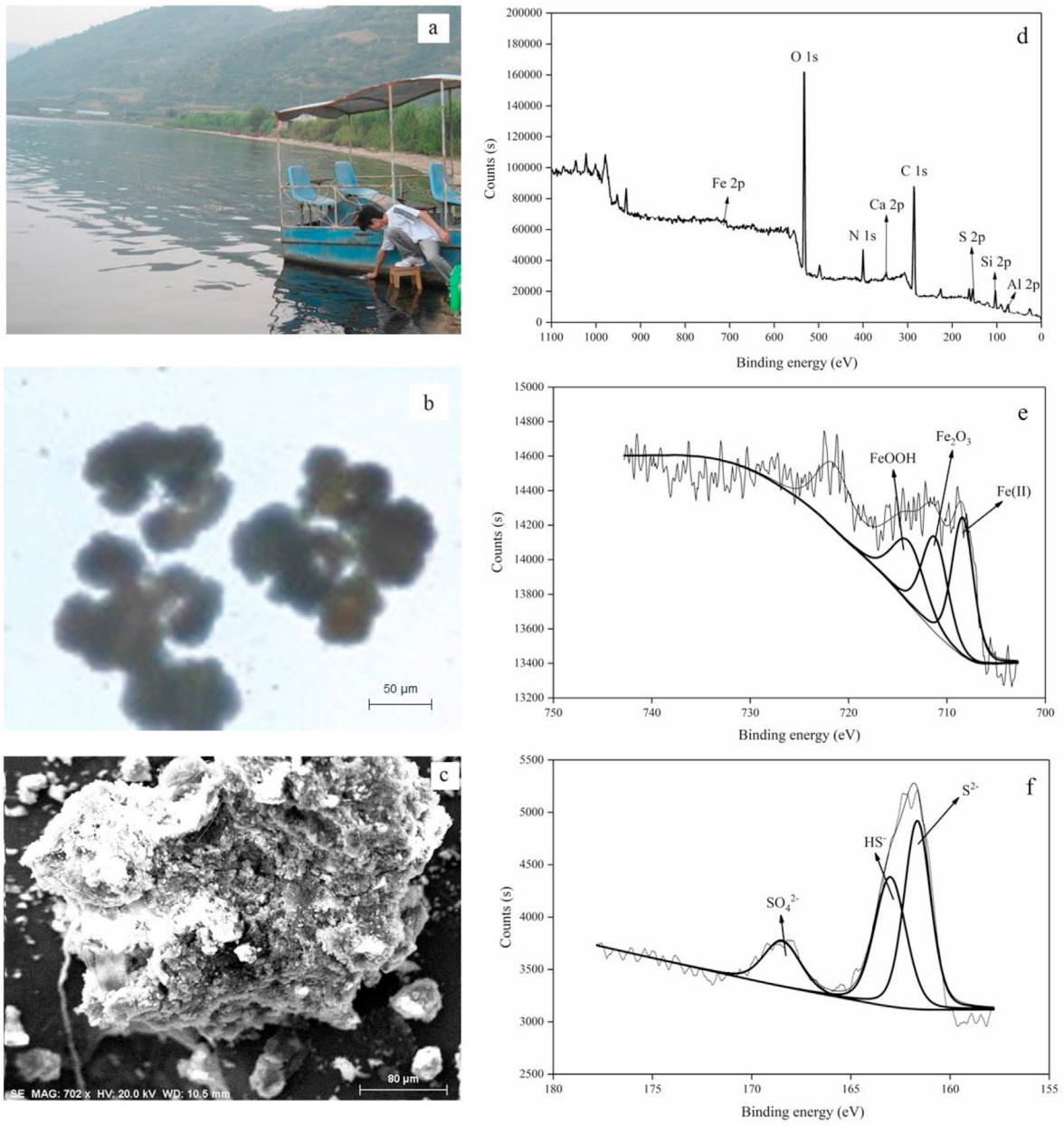

Fig. 1. Characteristics and composition of the black substances.

transects in the southern and northern lake zones (Fig. 2; Table S2). These sites are represented by "lake zone + approximate water depth". S20 is situated in the southern lake zone with a nearly 20 m depth and close to the Luju Estuary where agricultural wastewater and rainfull runoff flow into the lake. N45 is situated at the Dongda Estuary, where domestic sewage, waste residue of phosphorus rock and rainfull runoff drain into the lake through the river channel. Considering the steep slope of the lake bed, the chosen sites with different water depth can represent different organic matter content (Chen et al., 2018).

Black substances were sampled in surface water, and sediment cores were collected at each site in July 2016 by using a gravity core sampler equipped with a plexiglass tube (inner diameter of 110 mm). In N45, N150 and S80, additional sediment cores for CH_4 and porewater profiles (including NO_3^-, NO_2^-, NH_4^+ and SO_4^{2-}) were collected. All sediment cores were closed with rubber stoppers and transported to the laboratory within 4 h. After collecting, the samples for DO profiles and DGT measurement were immediately started. The samples for porewater profiles, Fe/S species and bag incubation were transferred into a N_2-filled glove bag, then top 6 cm of the sediment was sectioned into 1 cm intervals and the section from 6 cm to the bottom was sectioned into 2 cm intervals. After slicing, sub-samples at N45 and N150 with significantly different OM content, for bag incubation was initiated immediately. Sub-samples for porewater profiles were centrifuged and the supernatant was frozen at −20 °C after syringe filtration (0.45 μm). Sub-samples for Fe/S analysis were freeze-dried and homogenized in a mortar, then frozen at −20 °C.

2.2. Identification of the black substances

Black substances were firstly identified with microscopy (Zeiss

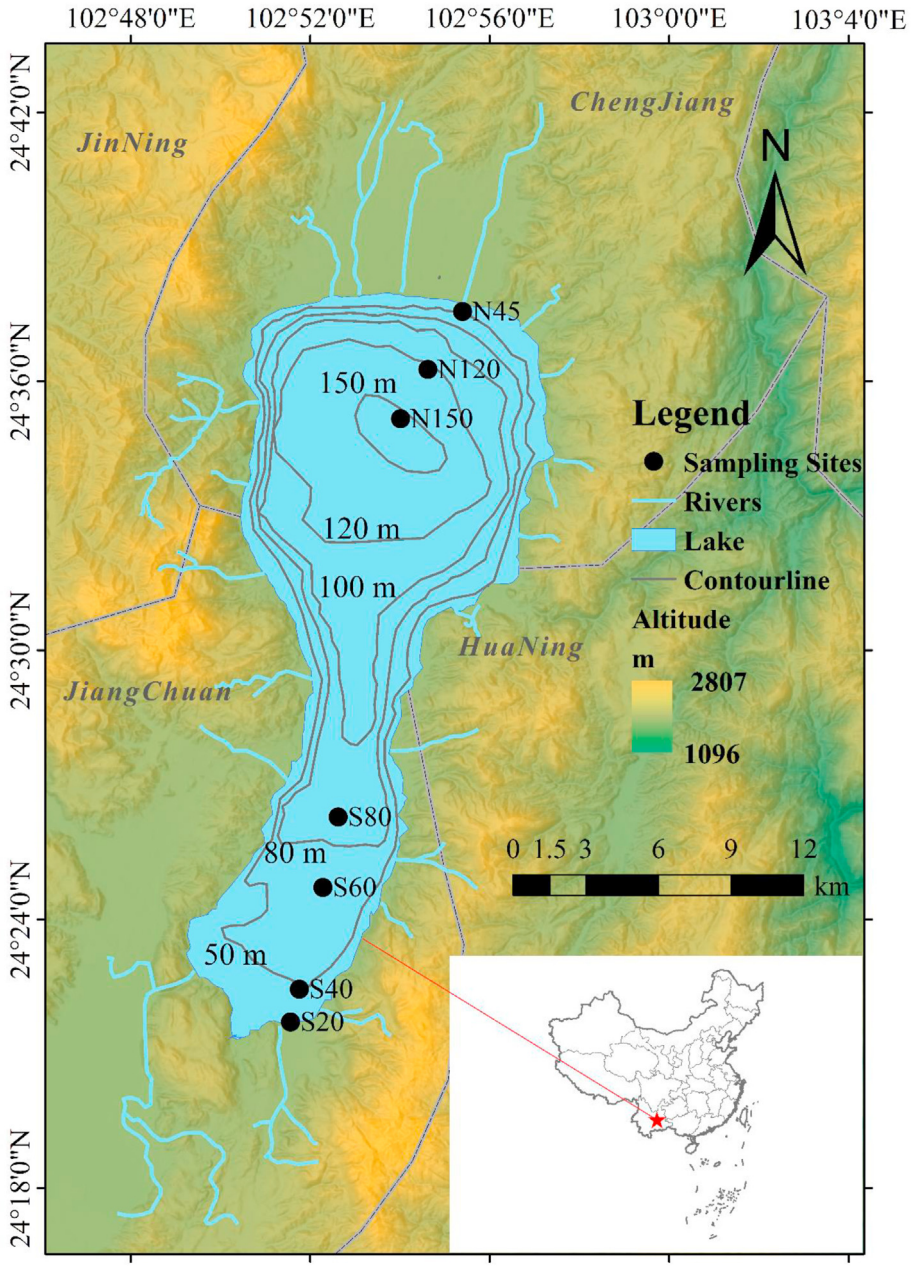

Fig. 2. Sampling sites in Lake Fuxian.

Stemi 508, Germany), and then the surface morphology and element composition were measured through scanning electron microscopy (SEM) model Zeiss EVO-18 with an Energy Dispersive Spectrometer (EDS) detector. In the SEM analysis, the samples were coated with a thin layer of gold. The accelerating voltage used was 20 KV, and the working distance was in the range of 10.5 mm. The chemical states of Fe 2p, Mn 2p and S 2p were determined for black substances by X-ray photoelectron spectroscopy (XPS) (ESCALAB 250, Thermo Fisher Scientific, USA). Because the components of the black substances were complex, the XPS analysis mainly presented the general information about element species. In addition, the homogenized freeze-dried black substance was digested with HNO_3—HF—$HClO_4$ in a Teflon beaker modified by Liu et al. (2014). Then the major and trace metal element contents were analyzed by Inductively Coupled Plasma Atomic Emission Spectrometry (ICP-AES, Teledyne Leeman Labs, Prodigy, USA) and inductively coupled plasma mass spectrometry (ICP-MS, Agilent 7700x, USA), respectively.

2.3. Dissolved oxygen (DO) profiles along sediments

A DO microelectrode (PreSens-Precision Sensing GmbH, Regensburg, Germany) was employed to measure sediment DO profiles with a 0.1 mm interval and each site was measured three times. The sediment-water interface (SWI) was identified by the inflection point of the DO-depth slope in the diffusion boundary layer. The oxygen penetration depth (OPD) and the oxygen consumption rate were identified by the PROFILE mode according to Berg et al. (1998).

2.4. Analysis of DGT-Fe^{2+}/S^{2-}/PO_4^{3-}

Diffusive gradients in thin films (DGT) is a dynamically passive sampling technique which is based on Fick's first law and has been widely applied to environmental monitoring and analytical chemistry (Davison and Zhang, 1994; Li et al., 2018). Two types of DGT devices, ZrO—AgI DGT and ZrO-Chelex DGT (Easy Sensor Ltd., Nanjing, China) were put into the sediments about 10 cm below the SWI. After 24 h, the DGT devices were retrieved to mark the SWI, then the S^{2-} and Fe^{2+}/PO_4^{3-} were analyzed. The details for analyzing the DGT probes were given in the Supplementary Information.

2.5. Determination of iron, sulfate reduction and anaerobic OM remineralization rates

In order to quantify the rate and relative contribution from various OM remineralization pathways along sediments, samples were incubated in gas-tight plastic bags modified by Hansen et al. (2000). The bag material is a transparent laminated plastic comprised of Nylon, ethylenevinyl alcohol, and polyethylene and has been proved with a low permeability for O_2 (Hansen et al., 2000). Here, two bags were used in order to keep the anaerobic conditions during every sampling, where the inner 10 × 10 cm bag was used to contain the sediments and the outer 30 × 30 cm bag was used to maintain an anaerobic environment (Fig S1).

Before the experiments initiated, the incubation bag was sealed with a hand-press heat sealer machine and the inner bag was evacuated by a vacuum pump. Then the sediments were purged with high-purity N_2 for 30 min, after which loading approximately 300 mL sediments into the inner bag via the sediment sampling hose. The sediments in the bag was pre-incubated for 48 h to remove the residual O_2, after which incubated in a constant temperature shaker with a dark state at 13 °C. At a certain time, 10 mL of sediment was sampled and centrifuged at 13 °C. After the supernatant was filtered by using the 0.45 μm filter membrane, 1 mL supernatant was sub-sampled to measure SO_4^{2-} and Fe^{2+}. The rest of the sediments were continued to be incubated after resealing. As for the CO_2 and CH_4 production rate, 3 mL of sediment was sampled by a 5 mL gas-tight syringe into a 20 mL serum vial, which was purged with high-purity nitrogen. Then the serum vials were immediately capped with butyl rubber stoppers and aluminum caps, subsequently shaken and kept at a constant temperature incubator of 13 °C. The serum vials were autoclaved at the same time as the bag incubations.

Iron reduction rates were calculated by regression of Fe^{2+} concentration along time and expressed in carbon equivalents according to the 1: 4 M ratio of CO_2 production: Fe^{2+} increase observed in the bag incubation experiment. Sulfate reduction rates were calculated by regression of SO_4^{2-} concentration along time and expressed in carbon equivalents according to the 2: 1 M ratio of CO_2 production: SO_4^{2-} decrease observed in the bag incubation experiment. Moreover, the sum of the CO_2 and CH_4 production rate was the total rate of OM remineralization (Thomsen et al., 2004; Chen and Jiang, 2016).

2.6. Chemical analytical methods

Porewater NO_3^-, NO_2^-, and NH_4^+ were measured using a continuous flow analyzer (San Plus, SKALAR, Netherlands), SO_4^{2-} was measured by using an ion chromatography (Dionex ICs2000, Sunnyvale, CA, USA). CO_2 and CH_4 concentration were determined via gas chromatography (Agilent 7890B, USA) equipped with a flame ionization detector (GC-FID) and a 3.66 high HayeSeq Q column with an inner diameter of 2 mm.

Acid volatile sulfide (AVS) and chromium reducible sulfide (CRS) in the sediments were successively extracted by the cold diffusion method with slight modifications (Hsieh and Shieh, 1997). After extraction, both AVS and CRS were determined by the Methylene blue spectrophotometric method (Ulrich et al., 1997). Amorphous ferrous oxides (L-Fe(II)) and ferric oxides (L-Fe(III)) in sediments were determined by using the Ferrozine method (Stookey, 1970). Total nitrogen (TN) and total organic carbon (TOC) of black substances and sediment samples were measured by a CHNS elemental analyzer (EA3000, EuroVector, Italy) according to Chen et al. (2018).

2.7. Statistical analysis

Statistical calculations were performed using Excel 2007. Correlation analysis with the corresponding figure and principal component analysis (PCA) were conducted using R 4.0.2 and one-way analysis of variance (ANOVA) analysis with the Tukey test were conducted using SPSS 22.0 software. A $p < 0.05$ was considered statistically significant different. The sampling site map was created using ArcGIS 10.2 software and the other figures were created in Origin 2017 software. In addition, Visual MINTEQ 3.1 model was applied to analyze the species of DGT-Fe^{2+} and show its transform in the porewater. The input data include pH, ferrous ion (DGT-Fe^{2+}), phosphorus (DGT-PO_4^{3-}), sulfur (DGT-S^{2-}), sulfate (SO_4^{2-}) and DOC (according to Chen et al., 2018). The DOC (SHM) model has been selected for the organic completion and the corresponding result was present in Supplementary Information.

3. Results

3.1. Identification of the black substances

According to the microscopy, the black substances were mainly composed of *Botryococcus braunii* (Fig. 1b) and SEM showed the blackness were irregular viscous agglomerations (Fig. 1c). EDS analysis revealed that C, O, Fe and S accounted for 62.6%, 29.8%, 0.45% and 0.14% without Mn existed which is in line with XPS analysis (Fig. 1d; Table S3; Fig S2). The XPS peaks of Fe 2p3/2 and Fe 2p1/2 are shown in Fig. 1e. Fe 2p3/2 can be divided into three main peaks appearing at 708 eV, 711 eV and 713 eV, associated with the binding energy of Fe atoms in Fe(II), Fe_2O_3 and FeOOH respectively (https://srdata.nist.gov/xps/selEnergyType.aspx), and Fe 2p1/2 appeared at 723 eV (Wang et al., 2016). The XPS peaks of S 2p can also be divided into three main peaks appearing at 161 eV, 163 eV and 168 eV (Fig. 1f), associated with the binding energy of S atoms in S^{2-}, HS^- and SO_4^{2-} respectively (Shchukarev et al., 2008). This confirmed the formation of FeS because the binding energy of S^{2-} was closed to FeS (161.6 eV) and much lower than that for FeS_2 (162.9 eV, Moulder et al., 1992). Element analysis further verified Fe was the dominant metal element with a concentration of 8063 mg/kg according to ICP-AES and ICP-MS (Table S3). In addition, TOC and TN of the black substances were 34.9% and 0.94%.

3.2. DO profile in sediments

DO not only decreased from the overlying water to the surface sediment along the depth in all sites but also decreased from the littoral to the pelagic zone at the SWI in both transects (Fig. 3a). Along the northern transect, DO at SWI decreased from 75.1 μM at N45 to 37.8 μM, the lowest value in all sites, at N150. Along the southern transect, DO at SWI deceased from 182 μM at S20 to 67.1 μM at S80. The range of OPD was 1.6—4.2 mm with no significant difference in any of the sites. The oxygen consumption rate was at the range of 0.03—0.18 nmol/cm^3/s, with the highest value at N45 and generally lower than 0.06 nmol/cm^3/s at the pelagic zone

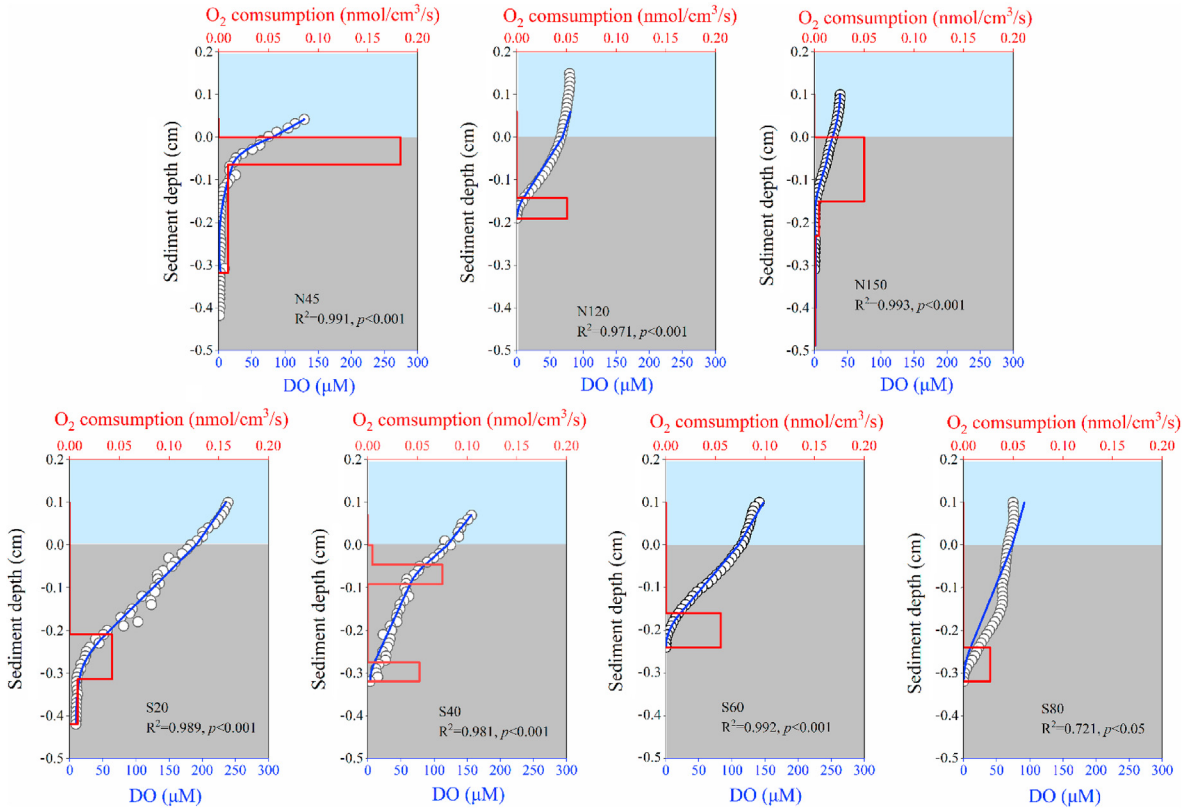

Fig. 3. (a) DO profile at the sediment-water interface (b) DGT-Fe^{2+}/PO_4^{3-} and average DGT-S^{2-} distribution along the sediment depth.

(N120, N150 and S80).

3.3. DGT-Fe^{2+}/S^{2-}/PO_4^{3-}

As shown in Fig. 3b, DGT-Fe^{2+} was below 1 μM in the overlying water and increased at the SWI to between 50 and 120 μM along the sediment depth. The DGT-Fe^{2+} then increased slowly or stabilized in all sites except for N150, where it failed to increase until reaching a depth of 30 mm below the SWI and subsequently kept increasing up to 269 μM along the depth. The DGT-Fe^{2+} at the pelagic zone (N120 and N150) was nearly 2.5 and 1.2 times higher than that at littoral zone (N45). A similar trend was also observed along the southern transect, where the DGT-Fe^{2+} was as high as 210 μM at the pelagic (S80), which was nearly double that at the littoral zone (S20 and S40). The species transfer of DGT-Fe^{2+} was shown in the Supplementary Information (Fig S3).

Similar trend was observed in vertical distribution of DGT-S^{2-} and DGT-PO_4^{3-}, which first increased along the sediment depth and then stabilized or slightly decreased after reaching its highest value (Fig. 3b, Fig S4). The depths with the highest value of DGT-S^{2-} in N120, N150, S60 and S80 were shallower at the SWI, 1.5 cm, 2 cm, and 1 cm below the SWI, respectively. However, the depth with the highest value of DGT-S^{2-} occurred in N45, S20 and S40 with relatively deeper positions at 3.2 cm, 7 cm, and 6.8 cm, respectively.

3.4. Porewater profile of SO_4^{2-}, NO_3^-, NO_2^-, NH_4^+ and dissolved CH_4

As shown in Fig S5, CH_4 concentration generally increased from the surface (57.5–808 μM) downward along the depth profile to the bottom and ranged from 931 μM to 2.30 mM. The concentration in N45 (1.53 ± 0.48 mM) was significantly higher than that in N150 and S80 ($p < 0.01$). SO_4^{2-} concentration generally decreased from the surface (261–389 μM) to depletion at the depth of 6 cm. NH_4^+ was only ranged from 0.35 to 0.76 mg/L but existed along upper 10 cm of the sediments. NO_3^- and NO_2^- were all below the detection limit.

3.5. Analysis of S and Fe species in sediments

The L-Fe(III) content stabilized between 10 and 60 μmol/gdw at the three sites of the northern transect and between 50 and 85 μmol/gdw at S60. At S20 and S80, the L-Fe(III) content decreased from 113 to 115 μmol/gdw at the surface sediment to 44.8–51 μmol/gdw at 10 cm below the SWI. As for the S40, the L-Fe(III) content fluctuatingly decreased from 195 μmol/gdw to 134 μmol/gdw at 10 cm below the SWI. The L-Fe(II) content increased slowly or stabilized from the surface sediment to the 10 cm below the SWI at all sites except for S40, where the L-Fe(II) content decreased initially and then stabilized between 180 and 230 μmol/gdw. Both L-Fe(III), L-Fe(II) and the total L-Fe were generally higher at sites S20 to S80 than those at N45 to N150 (Fig S6a).

AVS concentrations at all seven sites increased initially and then decreased along the sediment depth, reaching the maximum value of 0.65 μmol/gdw, 0.92 μmol/gdw, and 2.51 μmol/gdw at 4 cm, 1 cm, and 2 cm below the SWI at N45 to N150 and 0.01 μmol/gdw, 0.04 μmol/gdw, 0.03 μmol/gdw, and 0.68 μmol/gdw at 2 cm, 2 cm, 1 cm and 3 cm below the SWI at S20 to S80, respectively. The average AVS concentration in the top 10 cm sediments increased from the littoral to the pelagic zone in the northern and southern transect, respectively. In the northern transect, an average AVS concentration increased from 0.35 ± 0.18 μmol/gdw at N45 to 1.02 ± 0.89 μmol/

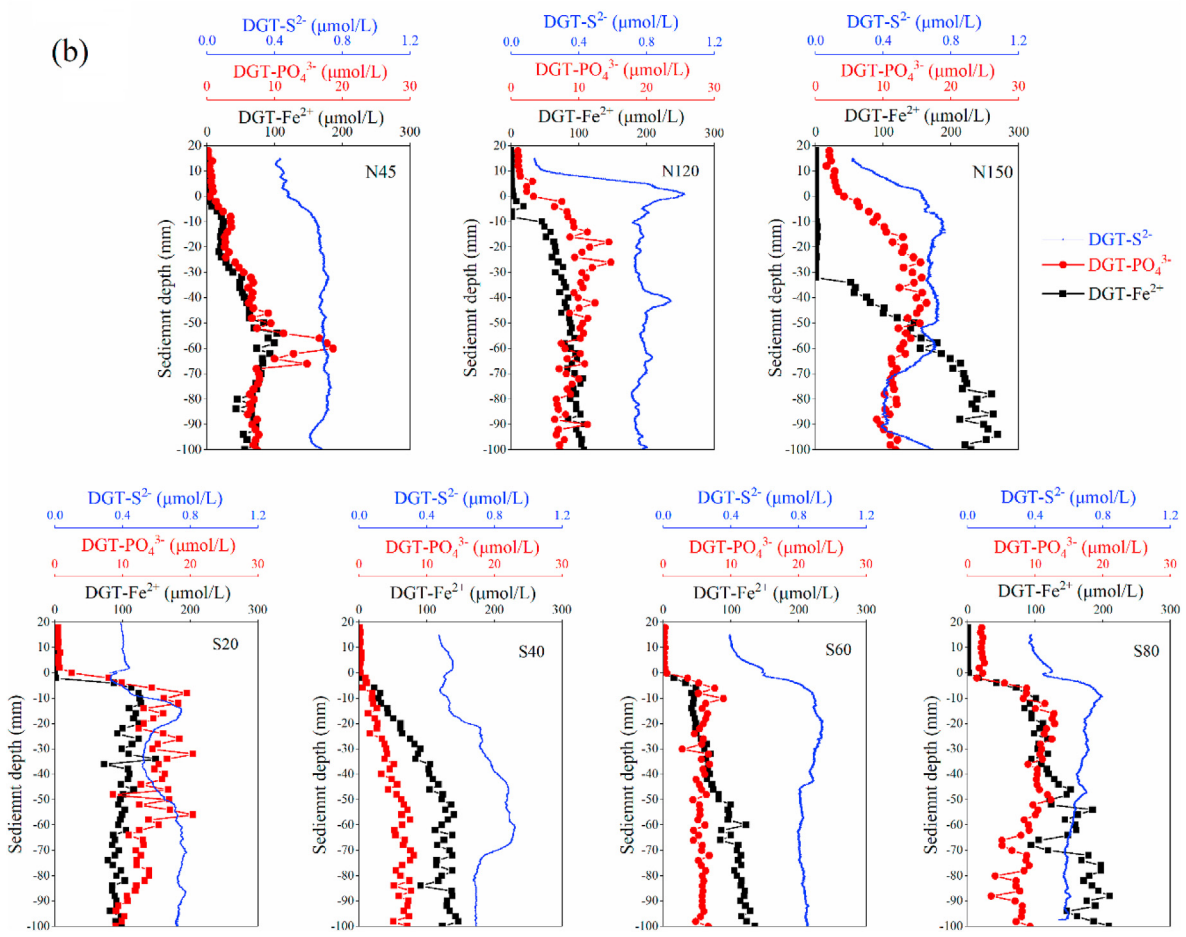

Fig. 3. (*continued*).

gdw at N150. As for the southern transect, the average AVS concentration increased from less than 0.01 μmol/gdw at S20 to 0.37 ± 0.19 μmol/gdw at S80. CRS concentration kept decreasing from 1.71 μmol/gdw at the surface to the bottom at N150. CRS concentrations at other six sample points (N45, N120 and S20, S40 S60, and S80) were similar to the vertical distribution of AVS, as they first increased and then decreased along depth, reaching the maximum value of 1.78 μmol/gdw, 1.31 μmol/gdw, 0.07 μmol/gdw, 0.19 μmol/gdw, 0.06 μmol/gdw and 0.02 μmol/gdw at 5 cm, 2 cm, 2 cm, 3 cm, 2 cm, and 1 cm below the SWI, respectively (Fig S6b).

3.6. Iron, sulfate reduction and anaerobic OM remineralization rate

Iron reduction rate (IRR), sulfate reduction rate (SRR) and methane production rate (MPR) co-existed at all layers of N45 and N150. The maximum value of IRR, SRR and MPR were 10.5, 3.86, and 146 nmol/cm^3/d, corresponding to the depth of 2–3 cm, 1–2 cm, and 2–3 at N45, and 6.71, 1.99, and 59.4 nmol/cm^3/d, corresponding to the depth of 2–3 cm, 0–1 cm and 3–4 cm at N150. The contribution of iron reduction and methane production to the OM remineralization was 1.65–8.78% and 33.1–74.9% at N45 as well as 2.34–17.1% and 3.62–60.2% at N150, respectively. However, the contributions of sulfate reduction to the OM remineralization were similar to the contributions at N45 and N150, which were 0.93–2.89% and 1.02–2.82% (Table S4).

4. Discussion

4.1. Composition of the black substances and its link to anaerobic OM remineralization

Black bloom phenomenon has been observed in many shallow lakes, and metal sulfide are the common responsible substance for the happening of black water (Cao et al., 2020; Feng et al., 2014; Han et al., 2015). Here we identified the black substances in a deep oligotrophic lake by using multiple microscopy and element analyses. Both EDS and XPS analysis showed that carbon and oxygen were the top two abundant elements among the black substances (Fig. 1d; Table S3), suggesting organic detritus is the main constituent. Specifically, microscopy showed a kind of phytoplankton *Botryococcus braunii* was existed in the black aggregates (Fig. 1b), but the ratio of TOC to TN was as high as 37.1, indicating terrestrial plant debris was also existed in the black substances (Gontharet et al., 2014). ICP-AES and ICP-MS measurements also showed that Fe concentration was 8063 mg/kg which was 13 times higher than that of Mn. XPS revealed that the area ratio of Fe(II) and S^{2-} account for 38.8% and 46.9% in Fe 2p and S 2p, and the binding energy of S^{2-} (161 eV) was closed to FeS (161.6 eV, Moulder et al., 1992), indicating FeS was the major cause for the blackness.

DO concentration at the SWI was at the range of 37.8-182 μM, indicating the water column in Lake Fuxian is permanently oxic, in line with our measurement in 2018 (Li et al., 2020). Some anaerobic

reduction process such as denitrification could happen in suspended solids which forms a micro-anoxic condition in the oxic water column (Klawonn et al., 2015, 2020). However, suspended solid in water column of Lake Fuxian is stable at 0.6–1.8 mg/L throughout the year (unpublished data), which is difficult to form such a large amount of FeS if iron and sulfate reduction could also happen in micro-anoxic conditions of the water column. Consequently, FeS is more likely formed in the sediment instead of permanently oxic water column.

Correlation analysis showed that TOC was significantly negatively correlated with the DO concentration at SWI (Fig S7). Sediment OM is a complex mixture of autochthonous material (generally composed of protein, lipids and carbohydrates) and allochthonous material (primarily composed of cellulose and structural compounds) (Chen et al., 2016). As the component of OM, especially autochthonous OM can be utilized by microbials, it is easily to result in DO depletion when OM travels downward to settle at the sediment-water interface. In accordance with many other lakes (Yu et al., 2017; Henrik et al., 1997; Kühl et al., 1998), the range of OPD at all sites was 1.6–4.2 mm, and the oxygen consumption rate was 0.03-0.18 nmol/cm^3/s (equal to 17280 nmol/cm^3/d), significantly higher than anaerobic OM remineralization pathways (Table S4), demonstrating DO was quickly consumed in the sediments of Lake Fuxian and anaerobic degradation is the major pathway to OM remineralization below several millimeter of the surface sediment. Moreover, FeS in the surface water is closely linked to anaerobic OM remineralization, especially iron and sulfate reduction in the sediment.

4.2. Coexistence of iron and sulfate reduction in sediment layers

Porewater profile showed that both NO_3^- and NO_2^- were below the detection limit, SO_4^{2-} existed in the upper 6 cm of the sediment, L-Fe(III) was always presented along the sediments but CH_4 was higher at the relatively deeper depth (Fig S5; Fig S6), suggesting OM remineralization coupled to iron, sulfate reduction and methanogenesis below the oxic surface sediments (Beulig et al., 2018; Thomsen 2004). From a thermodynamic perspective, the utilization of OM by iron reduction bacteria is prior to that by sulfate reduction bacteria due to competitive inhibition (Reeburgh, 1983; Thomsen 2004). However, in the upper 10 cm of the sediment porewater, DGT-Fe^{2+} and DGT-S^{2-} always coexisted which indicates that the iron and sulfate reduction occurred simultaneously in the sediment (Fig. 3b). In addition, the content of DGT-Fe^{2+} in porewater was 57.6–1919.4 times higher than that of DGT-S^{2-}, suggesting iron reduction exceeded sulfate reduction in all seven sites of Lake Fuxian. If sulfate reduction overrides iron reduction in the sediments, ferric oxides will directly be reduced by DGT-S^{2-} according to chemical iron reduction (CIR, Eq. (2)), which would produce solid FeS instead of such a large amount of dissolved DGT-Fe^{2+} (Ma et al., 2017).

DGT-Fe^{2+} were significantly negatively correlated with TOC or TN nearly at all sites (Fig. 4), indicating iron reduction was coupled to OM degradation. In sediments where microbial iron reduction (MIR) override chemical iron reduction (CIR), the phosphate adsorbed by ferric oxides is released into the porewater, so the simultaneous change of Fe^{2+} and PO_4^{3-} will occur (Ding et al., 2016; Mort et al., 2010). Here, DGT-Fe^{2+} also have a significantly positive correlation with DGT-PO_4^{3-} in all sites except for N150 (Fig. 4, Fig S8), which is in agreement with Lake Taihu (Ding et al., 2016), Lake Dongtinghu, Lake Chaohu and Lake Poyanghu (Gong et al., 2017), suggesting that the simultaneous change of Fe^{2+} and PO_4^{3-} is not only ubiquitous in the shallow lakes of the lower-middle reaches of the Yangtze River basin, but also applies to deep lakes in the Yunnan-Guizhou Plateau such as Lake Fuxian. Moreover, this study also confirms that DGT-S^{2-} has a significant and positive correlation with DGT-PO_4^{3-} in all sites (Fig. 4, Fig S8), which is attributed to the simultaneous reduction of both ferric oxides and sulfate as well as the associated release of Fe-bound P in sediments (Wang et al., 2015). Specifically, in the sediments where CIR overrides MIR, ferric oxides reduction couples with S^{2-} as the electron donor which is produced by SO_4^{2-} reduction, followed by FeS production; thus, the simultaneous change of S^{2-} and PO_4^{3-} occur. According to the bag incubation, both iron and sulfate reduction occurred along the upper 10 cm of sediments at N45 and N150. Iron reduction rate (IRR) were 1.96–10.5 and 1.69–6.71 nmol/cm^3/d at N45 and N150

Fig. 4. Correlation analysis among the chemical factors at different sites, wherein Fe^{2+}, S^{2-} and PO_4^{3-} denote to DGT-Fe^{2+}, DGT-S^{2-} and DGT-PO_4^{3-}, respectively.

respectively, which is significantly higher than the sulfate reduction rate (SRR). Collectively, iron and sulfate reduction coexisted in all the sediment layers but iron reduction was more important to OM remineralization relative to sulfate reduction.

4.3. Role of OM content on iron reduction and surface water blackness

PCA results showed that sites from the three northern sites and four southern sites were clustered, respectively. And TOC, AVS, TN, Fe(III) and Fe(II) were the major factors affected the variation among all the sampling sites (Fig S9), indicating OM is an important factor to cause the variation among the sites. Moreover, DGT-S^{2-} was significantly negatively correlated with TOC or TN at S20, S40 and N45 (Fig. 4), suggesting that sulfate reduction was coupled with OM degradation at these three OM-depleted sites. From the littoral to the pelagic sites, the negative correlation between DGT-S^{2-} and TOC weakened but the positive correlation between DGT-S^{2-} and Fe(II) at these pelagic sites were enhanced. This may result from transformation of organoclastic sulfate reduction at OM-depleted zones, to reaction of S^{2-} and Fe(III) at OM-rich zones. Correlation analysis also shows that the R^2 of DGT-Fe^{2+} to DGT-PO_4^{3-} was higher than that of DGT-PO_4^{3-} to DGT-S^{2-} at S20, S40 and N45 but lower at S60, S80, N120 and N150, suggesting that degree of CIR is higher at the four OM-rich sites (pelagic zone) than that at the three OM-depleted sites (littoral zone) (Fig. 4, Fig S8). Achtnich et al. (1995) found the increase of substrate content can promote the two reduction processes and alleviate the competition between iron and sulfate reduction. Structure of the microbial community may also be changed, especially that related to iron and sulfate reducing bacteria (Chen et al., 2020; Zhou et al., 2021). OM content was as high as 11.1% in the top 1 cm of the sediment layer and 4.29% in the upper 6 cm of the sediment layer in Lake Fuxian's pelagic zones (Table S2), significantly higher than some coastal and freshwater sediments where different OM remineralization pathways occurred simultaneously (Canfield et al., 1993; Motelica-Heino et al., 2003; Wu et al., 2016). Consequently, inhibition of sulfate reduction by ferric oxides was perhaps overcome as shown by the coexistence of iron and sulfate reduction as previously mentioned. Observations of CIR in low-sulfate environments have also been attributed to the presumed presence of highly crystalline ferric oxides (Bethke et al., 2011), but the content of amorphous ferric oxides reached nearly 120 μmol/gdw in this study (Fig S6a), which is poorly crystalline with high chemical reactivity. Hansel et al. (2015) found that sulfurization is still an important way to reduce iron even in a low sulfate environment (<1% sulfate concentration in the ocean) especially in OM rich zones, which agrees with our result.

Due to SO_4^{2-} and AVS was mainly presented in the upper 6 cm of the sediments, we calculate the average TOC values in this section and found the average TOC was significantly positively correlated with AVS (Fig S10, $R^2 = 0.95$, $p < 0.001$), further indicating that abundant OM contents is capable of facilitating chemical iron reduction which could enhance the formation of iron sulfide, thus contributing to the generation of black waters. AVS is the most active form of sulfur in sediment, including amorphous FeS (the major part), free sulfide, mackinawite, and other divalent metal sulfides (Hsieh and Shieh, 1997). In Lake Fuxian, the sulfate concentrations ranged between 200 and 500 μM (Fig S5), which are three orders of magnitude lower than that in the oceans, and iron reduction plays a more important role than sulfate reduction in OM remineralization as mentioned before, therefore, FeS formation is limited by sulfate reduction and AVS can represent a degree of chemical iron reduction (CIR) (Jorgensen et al., 2019). In April 2018, a serious *Aphanizomenon flos-aquae* bloom occurred in the northern basin of Lake Fuxian, causing TOC content was 1.5 times higher in 2018 than in this study (Li et al., 2020). Consequently, there will be a weakened competition between iron and sulfur reduction as well as more AVS produced and deteriorated water quality in hypolimnion layer if more OM input to the sediment continuously (Fig. 5). We estimate that AVS will increase 52% when increase 1%

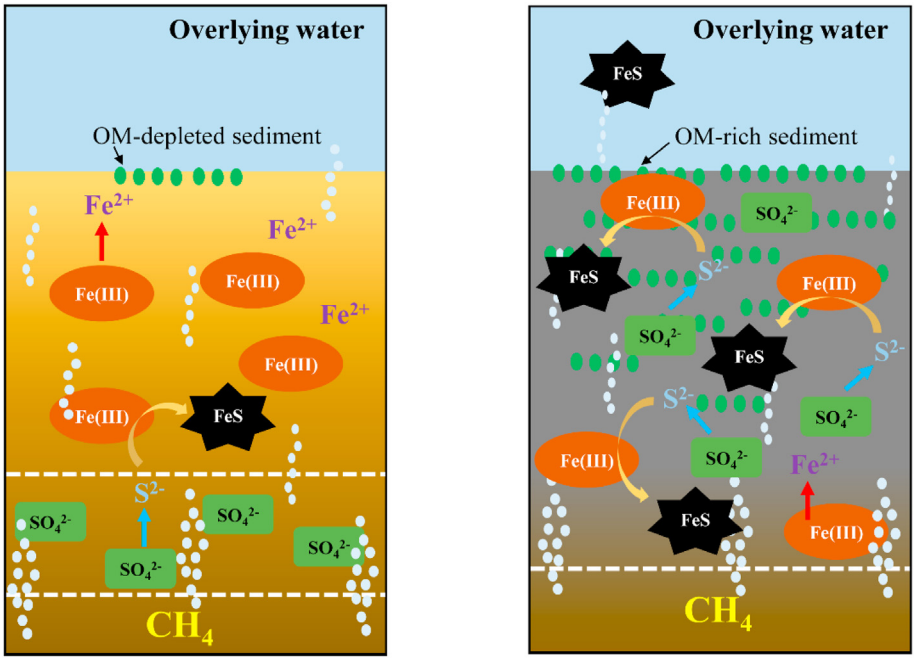

Fig. 5. Schematic diagram of iron reduction in OM-depleted and OM-rich sediments. In OM-depleted sediments, OM remineralization by iron reduction is prior to that by sulfate reduction due to competitive inhibition and Fe^{2+} is the major iron reduction product. However, abundant OM alleviate the competition between iron and sulfate reduction and even promote the coexistence of the two reduction processes. Consequently, FeS is the major iron reduction product as iron reduction coupled with S^{2-} produced by SO_4^{2-} reduction in OM-rich sediments. Potentially driven by CH_4 diffusion and turbulent flow, FeS transport upward from the sediment to the lake surface and form black bloom.

TOC/g sediment with the risk of surface water blackness appearance. However, how did these black substances travel from depth of near 100 m to the lake surface is still an interesting question. CH_4 flux at the SWI could reach to 1.69 mmol/m^2/d at N45 and 0.42–0.78 mmol/m^2/d, and accumulation of algae-derived OM lead to hypolimnion water hypoxia and higher methanogenesis potential (Li et al., 2020). We hypothesis that FeS may move up from the sediments to the water column by the upward diffusion of CH_4 and then adhere to the organic detritus, forming the visible blackness in the surface water under turbulent flow. Further research needs to focus on the occurrence conditions and influencing factors of black substances.

A recent study indicated that phytoplankton blooms intensity has increased in 68% of water bodies since the 1980s among 71 sites all over the world (Ho et al., 2019). Although surface water quality has been improved due to enormous investment in environmental remediation funded by the Chinese government (Zhou et al., 2017), sediment remediation in deep lakes has been constrained in China. Our study shows OM impact sediment iron and sulfur cycle and further result to blackness in surface water from a new sight. Management strategies including reducing the OM input and nutrient loads are very important to decrease primary production and prevent further deterioration of water quality in deep lakes such as Lake Fuxian. In addition, engineering strategies could also be used to increase DO artificially. Such strategies should include hypolimnetic aeration, hypolimnetic oxygenation, and hypolimnetic withdrawal to prevent AVS formation or promote AVS oxidation (Zhang et al., 2015a).

5. Conclusions

Collectively, the mechanism behind the black bloom in deep lakes was revealed by multiple elemental analysis and high-resolution geochemical investigations. The black substances were mainly composed of organic detritus (including *Botryococcus braunii* and terrestrial plant debris). Element analysis showed Fe was the dominant metal element with a concentration of 8063 mg/kg, indicating FeS was the major cause for surface water blackness which was further verified by XPS and EDS analysis. Dissolved oxygen penetrated 1.6–4.2 mm of the sediments, where anaerobic degradation played an important role in OM remineralization pathway and FeS formed. DGT profiles showed that DGT-Fe^{2+} concentration was 57.6–1919.4 times higher than the DGT-S^{2-} concentration and both were positively correlated with DGT-PO_4^{3-}, suggesting iron reduction and sulfate reduction co-existed in all sediment layers but iron reduction still overrode sulfate reduction which is further verified by bag incubation. Moreover, correlation of DGT-Fe^{2+} and DGT-PO_4^{3-} was better than that of DGT-PO_4^{3-} and DGT-S^{2-} at OM-depleted sites but opposite at OM-rich sites and total organic carbon (TOC) was significantly positively related to acid volatile sulfide (AVS). Therefore, abundant OM potentially could enhance chemical iron reduction and AVS production, which could further lead to black bloom in the water column. This study expands our knowledge of the effect of OM on sediment iron and sulfate reduction and its contribution to the black bloom. Moreover, both management and engineering strategies such as reducing the OM input and artificial aeration could be used to prevent the further deterioration of water quality in deep lakes such as Lake Fuxian.

Declaration of competing interest

The authors declare that they have no known competing financial interests or personal relationships that could have appeared to influence the work reported in this paper.

Acknowledgements

We would like to thank Jing Li, Shengrong Ding and Liujun Wang for their assistance in the field sampling and to Jingya Xue, Zhendu Mao, Yang Cheng and Peixin Gao for the help of figure modifications. We are particularly grateful to Dr. Changhui Wang for his kind help in XPS analysis. Our field work was also supported by The Fuxianhu Station of Plateau Deep Lake Research, NIGLAS. This work was supported by National Natural Science Foundation of China (grant numbers 41877482, 41471075), and the Project of Collabrative Innovation Center of Water Treatment Technology and Material.

Appendix A. Supplementary data

Supplementary data to this article can be found online at https://doi.org/10.1016/j.envpol.2020.116002.

References

Achtnich, C., Bak, F., Conrad, R., 1995. Competition for electron donors among nitrate reducers, ferric iron reducers, sulfate reducers, and methanogens in anoxic paddy soil. Biol. Fertil. Soils 19, 65–72. https://doi.org/10.1007/bf00336349.

Berberich, M.E., Beaulieu, J.J., Hamilton, T.L., Waldo, S., Buffam, I., 2019. Spatial variability of sediment methane production and methanogen communities within a eutrophic reservoir: importance of organic matter source and quantity. Limnol. Oceanogr. 64, 1–23. https://doi.org/10.1002/lno.11392.

Berg, P., Risgaard-Petersen, Nils, Rysgaard, S., 1998. Interpretation of measured concentration profiles in sediment pore water. Limnol. Oceanogr. 43, 1500–1510. https://doi.org/10.4319/lo.1998.43.7.1500.

Bethke, C.M., Sanford, R.A., Kirk, M.F., Jin, Q.S., Flynn, T.M., 2011. The thermodynamic ladder in geomicrobiology. Am. J. Sci. 311, 183–210. https://doi.org/10.2475/03.2011.01.

Beulig, F., Roy, H., Glombitza, C., Jorgensen, B.B., 2018. Control on rate and pathway of anaerobic organic carbon degradation in the seabed. Proc. Natl. Acad. Sci. U.S.A. 115, 367–372. https://doi.org/10.1073/pnas.1715789115.

Canfield, D.E., Thamdrup, B., Hansen, J.W., 1993. The anaerobic degradation of organic matter in Danish coastal sediments: iron reduction, manganese reduction, and sulfate reduction. Geochem. Cosmochim. Acta 57, 3867–3883. https://doi.org/10.1016/0016-7037(93)90340-3.

Cao, J.X., Sun, Q., Zhao, D.H., Xu, M.Y., Shen, Q.S., Wang, D., Wang, Y., Ding, S.M., 2020. A critical review of the appearance of black-odorous waterbodies in China and treatment methods. J. Hazard Mater. 385, 121511. https://doi.org/10.1016/j.jhazmat.2019.121511.

Chen, J., Xie, P., Yu, D.Z., Xie, L.J., Zeng, C., Chen, J., 2020. Dynamic change of sedimental microbial community during black bloom-an in situ enclosure simulation study. Microb Ecol. https://doi.org/10.1007/s00248-020-01561-2.

Chen, M., Jiang, H.L., 2016. Relative contribution of iron reduction to sediments organic matter mineralization in contrasting habitats of a shallow eutrophic freshwater lake. Environ. Pollut. 213, 904–912. https://doi.org/10.1016/j.envpol.2016.03.061.

Chen, M., Li, X.H., He, Y.H., Song, N., Cai, H.Y., Wang, C.H., Li, Y.T., Chu, H.Y., Krumholz, L.R., Jiang, H.L., 2016. Increasing sulfate concentrations result in higher sulfide production and phosphorous mobilization in a shallow eutrophic freshwater lake. Water Res. 96, 94–104. https://doi.org/10.1016/j.watres.2016.03.030.

Chen, X.C., Feng, M.H., Ke, F., Pan, J.Z., Fan, F., Wang, Y.R., Li, W.C., 2018. Source and biogeochemical distribution of organic matter in surface sediment in the deep oligotrophic lake fuxian, China. Aquat. Geochem. 24, 55–77. https://doi.org/10.1007/s10498-018-9330-5.

Chen, S., Liu, X.L., Song, Y.H., Liu, R.X., Gao, H.J., Han, L., Peng, J.F., 2017. Key blackening and stinking pollutants in Dongsha River of Beijing: spatial distribution and source identification. J. Environ. Manag. 200, 335–346. https://doi.org/10.1016/j.jenvman.2017.05.088.

Davison, W., Zhang, H., 1994. In situ speciation measurements of trace components in natural waters using thin-film gels. Nature 367, 546–548. https://doi.org/10.1038/367546a0.

Dean, J.F., Middelburg, J.J., Rockmann, T., Aerts, R., Blauw, L.G., Egger, M., Jetten, M.S.M., de Jong, A.E.E., Meisel, O.H., Rasigraf, O., Slomp, C.P., in't Zandt, M.H., Dolman, A.J., 2018. Methane feedbacks to the global climate system in a warmer world. Rev. Geophys. 56, 207–250. https://doi.org/10.1002/2017RG000559.

Ding, S.M., Wang, Y., Wang, D., Li, Y.Y., Gong, M.D., Zhang, C.S., 2016. In situ, high-resolution evidence for iron-coupled mobilization of phosphorus in sediments. Sci. Rep. 6, 24341. https://doi.org/10.1038/srep24341.

Duval, B., Ludlam, S.D., 2001. The black water chemocline of meromictic Lower Mystic Lake, Massachusetts. U.S.A. Int Rev Hydrobiol. 86, 165–181. https://doi.org/10.1002/1522-2632(200104)86:2<165::AID-IROH165>3.0.CO;2-Y.

Feng, Z.Y., Fan, C.X., Huang, W.Y., Ding, S.M., 2014. Microorganisms and typical

organic matter responsible for lacustrine “black bloom”. Sci. Total Environ. 470, 1–8. https://doi.org/10.1016/j.scitotenv.2013.09.022.
Freitag, T.E., Klenke, T., Krumbein, W.E., Gerdes, G., Prosser, J.I., 2003. Effect of anoxia and high sulphide concentrations on heterotrophic microbial communities in reduced surface sediments (Black Spots) in sandy intertidal flats of the German Wadden Sea. FEMS Microbiol. Ecol. 44, 291–301. https://doi.org/10.1016/S0168-6496(03)00076-X.
Gontharet, S., Mathieu, O., Lévêque, J., Milloux, M.J., Lesourd, S., Philippe, S., Cailaud, J., Gardel, A., Sarrazin, M., Proisy, C., 2014. Distribution and sources of bulk organic matter (OM) on a tropical intertidal mud bank in French Guiana from elemental and isotopic proxies. Chem. Geol. 376, 1–10. https://doi.org/10.1016/j.chemgeo.2014.03.009.
Gong, M.D., Jin, Z.F., Wang, Y., Lin, J., Ding, S.M., 2017. Coupling between iron and phosphorus in sediments of shallow lakes in the middle and lower reaches of Yangtze River using diffusive gradients in thin films (DGT). J. Lake Sci. 29, 1103–1111. https://doi.org/10.18307/2017.0508 (In Chinese).
Han, C., Ding, S.M., Yao, L., Shen, Q.S., Zhu, C.G., Wang, Y., et al., 2015. Dynamics of phosphorus-iron-sulfur at the sediment-water interface influenced by algae blooms decomposition. J. Hazard Mater. 300, 329–337. https://doi.org/10.1016/j.jhazmat.2015.07.009.
Hansel, C.M., Lentini, C.J., Tang, Y.Z., Johnston, D.T., Wankel, S.D., Jardine, P.M., 2015. Dominance of sulfur-fueled iron oxide reduction in low-sulfate freshwater sediments. ISME J. 15, 1–13. https://doi.org/10.1038/ismej.2015.1050.
Hansen, J.W., Thamdrup, B., Jørgensen, B.B., 2000. Anoxic incubation of sediment in gas-tight plastic bags: a method for biogeochemical process studies. Mar. Ecol. Prog. Ser. 208, 273–282. https://doi.org/10.3354/meps208273.
Henrik, S., Heribert, C., Hans-Dietrich, B., 1997. Vertical distribution of sulfate-reducing bacteria at the oxic-anoxic interface in sediments of the oligotrophic Lake Stechlin. FEMS Microbiol. Ecol. 22, 245–255. https://doi.org/10.1111/j.1574-6941.1997.tb00377.x.
Ho, J.C., Michalak, A.M., Pahlevan, N., 2019. Widespread global increase in intense lake phytoplankton blooms since the 1980s. Nature 574, 667–670. https://doi.org/10.1038/s41586-019-1648-7.
Hsieh, Y.P., Shieh, Y.N., 1997. Analysis of reduced inorganic sulfur by diffusion methods: improved apparatus and evaluation for sulfur isotopic studies. Chem. Geol. 137, 255–261. https://doi.org/10.1016/S0009-2541(96)00159-3.
Huisman, J., Codd, G.A., Paerl, H.W., Ibelings, B.W., Verspagen, J.M.H., Visser, P.M., 2018. Cyanobacterial blooms. Nat Rev Microbial 16, 471–483. https://doi.org/10.1038/s41579-018-0040-1.
Jorgensen, B.B., Findlay, A.J., Pellerin, A., 2019. The biogeochemical sulfur cycle of marine sediments. Front. Microbiol. 10, 849. https://doi.org/10.3389/fmicb.2019.00849.
Klawonn, I., Bonaglia, S., Brüchert, V., Ploug, H., 2015. Aerobic and anaerobic nitrogen transformation processes in N_2-fixing cyanobacterial aggregates. ISME J. 9, 1456–1466. https://doi.org/10.1038/ismej.2014.232.
Klawonn, I., Eichner, M.J., Wilson, S.T., Moradi, N., Thamdrup, B., Kummel, S., Gehre, M., Khalili, A., Grossart, H.P., Karl, D.M., Ploug, H., 2020. Distinct nitrogen cycling and steep chemical gradients in Trichodesmium colonies. ISME J. 14, 399–412. https://doi.org/10.1038/s41396-019-0514-9.
Kühl, M., Steuchart, C., Eickert, G., Jeroschewski, P., 1998. A H_2S microsensor for profiling biofilms and sediments: application in an acidic lake sediment. Aquat. Microb. Ecol. 15, 201–209. https://doi.org/10.3354/ame015201.
Li, B., Gu, Q.J., Miao, Y.Q., Luo, W.L., Xing, P., Wu, Q.L., 2020. Methane distribution patterns along a transect of Lake Fuxian, a deep oligotrophic lake in China. Environ. Sci. Pollut. Res. 27, 25848–25860. https://doi.org/10.1007/s11356-019-06098-7.
Li, C., Ding, S.M., Yang, L.Y., Wang, Y., Ren, M.Y., Chen, M.S., Fan, X.F., Lichtfouse, E., 2018. Diffusive gradients in thin films: devices, materials and applications. Environ. Chem. Lett. 17, 801–831. https://doi.org/10.1007/s10311-018-00839-9.
Liu, C., Shen, Q.S., Zhou, Q.L., Fan, C.X., Shao, S.G., 2015. Precontrol of algae-induced black blooms through sediment dredging at appropriate depth in a typical eutrophic shallow lake. Ecol. Eng. 77, 139–145. https://doi.org/10.1016/j.ecoleng.2015.01.030.
Liu, E.F., Shen, J., 2014. A comparative study of metal pollution and potential eco-risk in the sediment of Chaohu Lake (China) based on total concentration and chemical speciation. Environ. Sci. Pollut. Res. 21, 7285–7295. https://doi.org/10.1007/s11356-014-2639-8.
Lovley, D.R., 1987. Organic matter mineralization with the reduction of ferric iron: a review. Geomicrobiol. J. 5, 375–399. https://doi.org/10.1080/01490458709385975.
Ma, W.W., Mao, M.X., Yang, G.P., Li, T., 2017. In situ, high-resolution DGT measurements of dissolved sulfide, iron and phosphorus in sediments of the East China Sea: insights into phosphorus mobilization and microbial iron reduction. Mar. Pollut. Bull. 124, 400–410. https://doi.org/10.1016/j.marpolbul.2017.07.056.
Mahmoudi, N., Enke, T.N., Beaupre, S.R., Teske, A.P., Cordero, O.X., Pearson, A., 2020. Illuminating microbial species-specific effects on organic matter remineralization in marine sediments. Environ. Microbiol. 22, 1734–1747. https://doi.org/10.1111/1462-2920.14871.
Melton, E.D., Swanner, E.D., Behrens, S., Schmidt, C., Kappler, A., 2014. The interplay of microbially mediated and abiotic reactions in the biogeochemical Fe cycle. Nat Rev Microbial 12, 797–808. https://doi.org/10.1038/nrmicro3347.
Mort, H.P., Slomp, C.P., Gustafsson, B.G., Andersen, T.J., 2010. Phosphorus recycling and burial in Baltic Sea sediments with contrasting redox conditions. Geochem. Cosmochim. Acta 74, 1350–1362. https://doi.org/10.1016/j.gca.2009.11.016.
Motelica-Heino, M., Naylor, C., Zhang, H., Davison, W., 2003. Simultaneous release of metals and sulfide in lacustrine sediment. Environ. Sci. Technol. 37, 4374–4381. https://doi.org/10.1021/es030035+.
Moulder, J.F., Stickle, W.F., Sobol, P.E., Bomben, K.D., 1992. Handbook of X-Ray Photoelectron Spectroscopy: a Reference Book of Standard Spectra for Identification and Interpretation of XPS Data. Perkin-Elmer Corp., Physical Electronics Division: Eden Prairie, MN.
Nanjing Institute of Geography and Limnology, 1990. Lake Fuxian. Ocean Press, Beijing (In Chinese).
Qin, B.Q., Zhou, J., Elser, J.J., Gardner, W.S., Deng, J.M., Brookes, J.D., 2020. Water depth underpins the relative roles and fates of nitrogen and phosphorus in lakes. Environ. Sci. Technol. 54, 3191–3198. https://doi.org/10.1021/acs.est.9b05858.
Reeburgh, W.S., 1983. Rates of biogeochemical processes in anoxic sediments. Annu. Rev. Earth Planet Sci. 11, 269–298. https://doi.org/10.1146/annurev.ea.11.050183.001413.
Shen, Q.S., Liu, C., Zhou, Q.L., Shang, J.G., Zhang, L., Fan, C.X., 2013. Effects of physical and chemical characteristics of surface sediments in the formation of shallow lake algae-induced black bloom. J. Environ. Sci. 25, 2353–2360. https://doi.org/10.1016/S1001-0742(12)60325-8.
Shchukarev, A., Galman, V., Rydberg, J., Sjoberg, S., Renberg, I., 2008. Speciation of iron and sulphur in seasonal layers of varved lake sediment: an XPS study. Surf. Interface Anal. 40, 354–357. https://doi.org/10.1002/sia.2704.
Stookey, L.L., 1970. Ferrozine - a new spectrophotometric reagent for iron. Anal. Chem. 42, 779–781. https://doi.org/10.1021/ac60289a016.
Thomsen, U., Thamdrup, B., Stahl, D.A., Canfield, D.E., 2004. Pathways of organic carbon oxidation in a deep lacustrine sediment, Lake Michigan. Limnol. Oceanogr. 49, 2046–2057. https://doi.org/10.4319/lo.2004.49.6.2046.
Ulrich, G.A., Krumholz, L.R., Suflita, J.M., 1997. A rapid and simple method for estimating sulfate reduction activity and quantifying sulfides. Appl. Environ. Microbiol. 63, 1627–1630. https://doi.org/10.1128/AEM.63.4.1627-1630.1997.
Wang, C.H., Jiang, H.L., Yuan, N.N., Pei, Y.S., Yan, Z.S., 2016. Tuning the adsorptive properties of drinking water treatment residue via oxygen-limited heat treatment for environmental recycle. Chem. Eng. J. 284, 571–581. https://doi.org/10.1016/j.cej.2015.09.011.
Wang, G.F., Li, X.N., Fang, Y., Huang, R., 2014. Analysis on the formation condition of the algae-induced odorous black water agglomerate. Saudi J. Biol. Sci. 21, 597–604. https://doi.org/10.1016/j.sjbs.2014.07.002.
Wang, Y.P., Guan, Q.W., Li, C., Xu, D., Ding, S.M., 2015. A study of in situ synchronous measurement of available phosphorus and surfur in the sediments of Lake Chaohu by diffusive gradients in thin films (DGT). Acta Scientiae Circumstantiae 35, 2512–2518. https://doi.org/10.13671/j.hjkxxb.2014.0996 (In Chinese).
Wu, Z.H., Jiao, L.X., Wang, S.R., 2016. The measurement of phosphorus, sulfide and metals in sediment of Dianchi Lake by DGT (diffusive gradients in thin films) probes. Environ Earth Sci 75, 193. https://doi.org/10.1007/s12665-015-4978-2.
Yu, J.H., Ding, S.M., Zhong, J.C., Fan, C.X., Chen, Q.W., Yin, H.B., Zhang, L., Zhang, Y.L., 2017. Evaluation of simulated dredging to control internal phosphorus release from sediments: focused on phosphorus transfer and resupply across the sediment-water interface. Sci. Total Environ. 592, 662–673. https://doi.org/10.1016/j.scitotenv.2017.02.219.
Zhang, Y.L., Wu, Z.X., Liu, M.L., He, J.B., Shi, K., Zhou, Y.Q., Wang, M.Z., Liu, X.H., 2015a. Dissolved oxygen stratification and response to thermal structure and long-term climate change in a large and deep subtropical reservoir (Lake Qiandaohu, China). Water Res. 75, 249–258. https://doi.org/10.1016/j.watres.2015.02.052.
Zhang, Y.D., Su, Y.L., Liu, Z.W., Chen, X.C., Yu, J.L., Di, X.D., Jin, M., 2015b. Sediment lipid biomarkers record increased eutrophication in Lake Fuxian (China) during the past 150 years. J. Great Lake. Res. 41, 30–40. https://doi.org/10.1016/j.jglr.2014.11.025.
Zhao, X.Q., Miao, P.P., Pu, J.W., Li, S.N., Wang, Q., Tan, K., Lu, F.F., Yi, Q., 2020. Land use change and its impact on the gross ecosystem product in Fuxian Lake Basin. Res. Soil Water Conserv. 27, 291–299 (In Chinese).
Zhou, C., Miao, T., Jiang, L., Zhang, H., Zhang, Y., Zhang, X., 2021. Conditions that promote the formation of black bloom in aquatic microcosms and its effects on sediment bacteria related to iron and sulfur cycling. Sci. Total Environ. 751, 141–869. https://doi.org/10.1016/j.scitotenv.2020.141869.
Zhou, Y.Q., Ma, J.R., Zhang, Y.L., Qin, B.Q., Jeppesen, E., Shi, K., Brookes, J.D., Spencer, R.G.M., Zhu, G.W., Gao, G., 2017. Improving water quality in China: environmental investment pays dividends. Water Res. 118, 152–159. https://doi.org/10.1016/j.watres.2017.04.035.
Zhou, Y.Q., Xiao, Q.T., Yao, X.L., Zhang, Y.L., Zhang, M., Shi, K., Lee, X.H., Podgorski, D.C., Qin, B.Q., Spencer, R.G.M., Jeppesen, E., 2018. Accumulation of terrestrial dissolved organic matter potentially enhances dissolved methane levels in eutrophic Lake Taihu, China. Environ. Sci. Technol. 52, 10297–10306. https://doi.org/10.1021/acs.est.8b02163.